Arab J Sci Eng (2015) 40:2261–2269
DOI 10.1007/s13369-015-1748-0

RESEARCH ARTICLE - CIVIL ENGINEERING

Thermal Behavior of Portland Cement and Fly Ash–Metakaolin-Based Geopolymer Cement Pastes

Ping Duan[1,2,3] · **Chunjie Yan**[1,2,3] · **Wei Zhou**[1,2] · **Wenjun Luo**[1,2]

Received: 14 January 2015 / Accepted: 8 June 2015 / Published online: 27 June 2015

Abstract Geopolymer specimens were prepared by combination of fly ash and metakaolin activated by sodium silicate (Na_2SiO_3) and sodium hydroxide (NaOH) solutions. The effect of high temperature on the compressive strength, mass loss and shrinkage of geopolymer cement pastes and ordinary portland cement (OPC) pastes were assessed experimentally. Microstructure formation and development were characterized in terms of pore structure by mercury intrusion porosimetry. The results reveal that at temperatures exceeding 400 °C geopolymer cement paste is superior to OPC paste. Firstly, the compressive strength drops rapidly for the OPC paste to practically zero strength at 600 °C, while it drops slowly for the fly ash–metakaolin-based geopolymer cement paste to 46 MPa at 1000 °C. Secondly, while the mass loss increases for the OPC paste, it is maintained at a constant, lower value for the geopolymer cement paste. Thirdly, shrinkage of geopolymer cement paste is at least three times smaller than that of OPC paste.

Keywords Thermal properties · Cement · Geopolymer · Fly ash · Metakaolin

✉ Chunjie Yan
chjyan2005@126.com

[1] Faculty of Materials Science and Chemistry, China University of Geosciences, Wuhan 430074, China

[2] Engineering Research Center of Nano-Geomaterials of Ministry of Education, China University of Geosciences, Wuhan 430074, China

[3] Zhejiang Research Institute, China University of Geosciences, Hangzhou 311305, China

1 Introduction

Cement industry is acknowledgedly associated with the large amount of CO_2 emission. Accordingly, development of alternative cementitious materials from by-products including slag, fly ash and bottom ash is considered existing strategy to reduce the CO_2 emission of concrete industry. Geopolymers are considered to be one of these alternative cementitious materials with widely potential application value in cement and concrete due to its high early strength and excellent durability as well as reduced CO_2 emission [1–3]. Based on the properties mentioned above, researchers are showing wide interest in geopolymer binders, i.e., the alkali activated binders with metakaolin or fly ash precursors. However, the literature on portland cement and geopolymer exposed to high temperature at about 1000 °C is scant [1–7]. Therefore, this paper provides a comparison of high-temperature-exposed pastes of OPC and geopolymer comprised of fly ash, metakaolin and sodium silicate (Na_2SiO_3) and sodium hydroxide (NaOH) solutions. Compressive strength, mass loss and shrinkage as a function of firing temperature were compared. Microstructure formation and development were characterized in terms of pore structure by mercury intrusion porosimetry (MIP).

2 Materials

Fluidized bed fly ash was provided by Shenhua Junggar Energy Corporation in Junggar, Inner Mongolia, China. Metakaolin was obtained from Yunnan, China. Their chemical compositions are provided in Table 1.

Portland cement (CEM O 42.5) having relative density 3100 kg/m^3 (relative density is the ratio of the mass of a unit volume of cement to the density of a given reference

Table 1 Chemical compositions of raw materials by X-ray fluorescence (XRF) analysis (mass, %)

	SiO_2	Al_2O_3	Fe_2O_3	MgO	CaO	Na_2O	K_2O	MnO	TiO_2	LOI
Cement	21.35	7.67	3.31	3.08	62.60	0.35	0.39	0.05	0.25	0.95
Fly ash	29.47	51.72	2.25	0.15	5.21	0.05	0.35	0.03	1.83	8.58
Metakaolin	53.32	42.09	2.33	0.21	0.09	0.49	0.64	0.02	0.63	0.08

Table 2 Properties of cement paste having water/cement ratio = 0.5

Compressive strength (MPa)[a]		Flexural strength (MPa)[b]		Initial setting time (min)[c]	Final setting time (min)[c]
3 days	28 days	3 days	28 days		
27.3	47.5	6.3	8.7	132	187

[a] Compressive strength of geopolymer paste and OPC samples was performed according to ASTM C109 [5]. For each mix, six specimens were used and the average of these three values was reported
[b] The flexural strength test was performed on dried specimens in accordance with ASTM C348-08 [6]
[c] In fresh pastes, the initial and final setting time was determined using the Vicat apparatus in accordance with the ASTM C191 [7] standard test method

material, usually with respect to water), specific surface area 369.6 m^2/kg (specific surface area is a property of cement which is the total surface area per unit of mass), chemical composition as shown in Table 1 and strength and setting properties as shown in Table 2 was used.

Scanning electron microscopic (SEM) study of the fly ash and metakaolin reveals some interesting features related to the morphology of fly ash and metakaolin samples. Figures 1 and 2 indicate the geometrical properties of the former two materials, respectively; it can be seen that shape is usually irregular and appears to be porous in a potential state of fragmentation with small and rough particles. Metakaolin shows the presence of very fine particles with size of approximately 10 μm being perceived as an agglomeration of particles. However, the distribution of particle sizes is different for flocculated and plate-shaped fly ash, and the largest particles are approximately 30 μm in size.

The alkali activator is composed of sodium silicate and sodium hydroxide (99.2 % NaOH) in analytical reagent degree. The liquid portions in the mixture are 10 M sodium

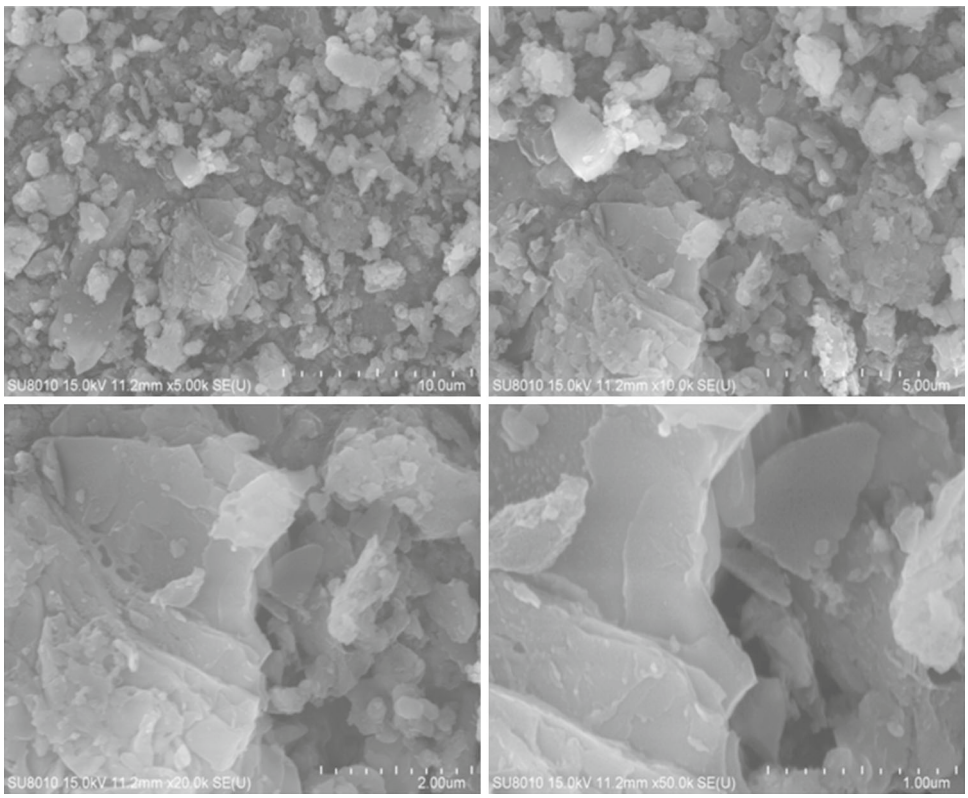

Fig. 1 Micrographs of fluidized bed fly ash by scanning electron microscope (SEM)

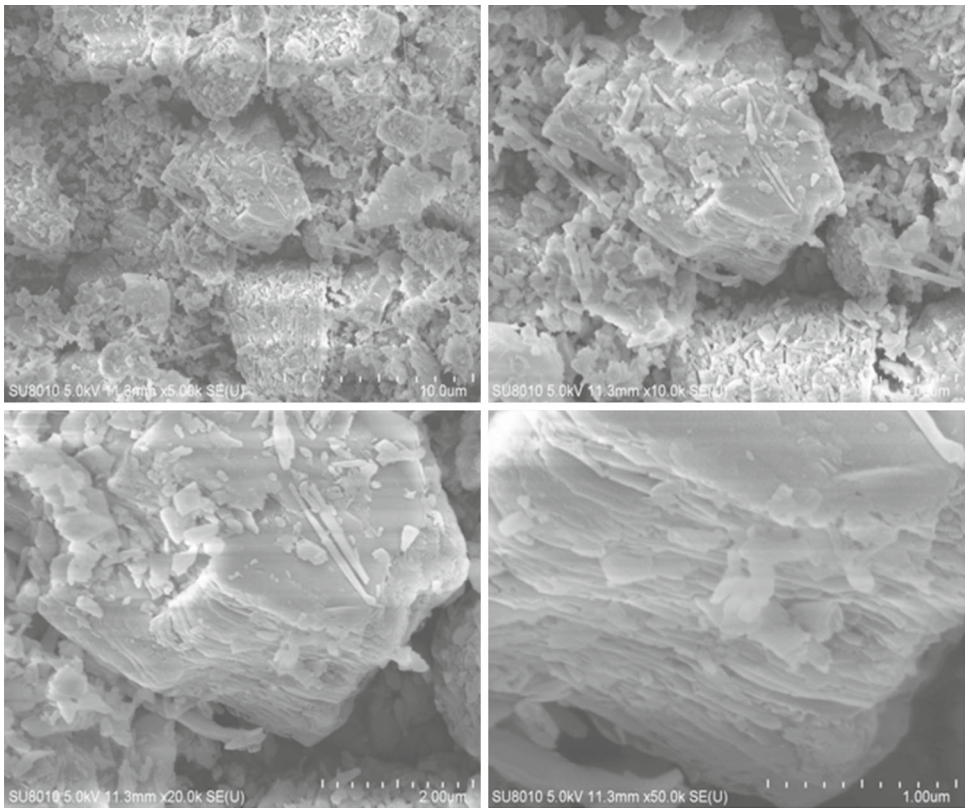

Fig. 2 Micrographs of metakaolin by scanning electron microscope (SEM)

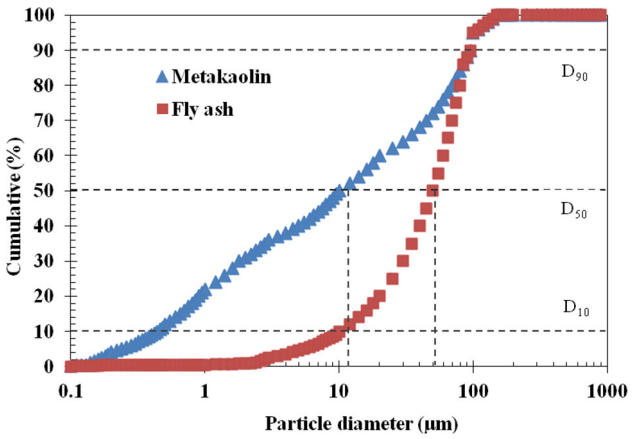

Fig. 3 Particle size distribution of FA and MK samples

hydroxide (NaOH) and sodium silicate (Na_2SiO_3) with 14.51 % Na_2O, 33.39 % SiO_2 and 48.53 % H_2O.

The particle size analysis of fly ash and metakaolin were carried out using a laser diffraction particle size analyzer (MASTERSIZER S, Malvern, UK). Subsequently, each sample was grinded and sieved for 30 min in a sieve shaker using sieves no. 300. Each of the size fractions so obtained was separately analyzed for particle size distribution. Sieve analysis of fly ash and metakaolin reveals that the particle size range varies widely.

Table 3 Particle diameter of fly ash and metakaolin samples (μm)

Characteristic diameter	Fly ash	Metakaolin
D_{90}	103.53	99.87
D_{50}	51.09	12.66
D_{10}	10.31	0.49

Figure 3 shows the particle size distribution of fly ash and metakaolin samples. The characteristic particle diameters D_{10}, D_{50} and D_{90} are tabulated in Table 3. A wide variation in particle size was observed in the fly ash–metakaolin. In metakaolin, 90 % particles were <100 μm size, whereas in fly ash, the coarser size just exceeded 100 μm.

Geopolymer samples were synthesized by alkaline activation of combination of fly ash and metakaolin with mass ratios of 1:1 with silicate solutions (modulus of water glass, MR = 1.5). The liquid/solid (L/S) mass ratio is kept constant at 0.5, the liquid comprising water in alkaline solutions and the extra water and the solid materials comprising fly ash, metakaolin or a combination of them.

The activating solutions were prepared by mixing sodium hydroxide (analytical grade, >99 % purity) with distilled water and sodium silicate solution. All activating solutions were prepared one day before the sample preparation. Mixture proportions for geopolymer and OPC are listed in Table 4. The cement paste used in this study was CEM O 42.5. The water/cement ratio was kept constant at 0.5.

Table 4 Mixture proportions of geopolymer and OPC pastes

Sample	Fly ash (g)	Metakaolin (g)	Cement (g)	SiO_2 (mol)	Na_2O (mol)	H_2O (g)
Geopolymer	500	500	0	1.5	1.0	500
Fly ash geopolymer	1000	0	0	1.5	1.0	500
Metakaolin geopolymer	0	1000	0	1.5	1.0	500
OPC	0	0	1000	0	0	500

Fresh geopolymer pastes and cement paste were cast in triplet steel molds of 40 mm × 40 mm × 40 mm cubes and vibrated to remove entrained air bubbles. The molds were then sealed with polyethylene film and set into a standard curing box. After initial curing at 40 °C for 1 day, the samples were demolded and subjected to further curing at 40 °C for 28 days.

3 Experimental Technique

Compressive strength tests were performed on cubes using a universal testing machine with a loading rate of 0.6 MPa/s at age of 3, 7 and 28 days after casting the samples at 20 °C followed by curing at 40 °C for 24 h. Averages of six samples were tested for each result. For each age, six specimens were tested and the mean value of these measurements is reported. Compressive strength of OPC and geopolymer pastes was determined by standard uniaxial compressive test using universal testing device. The tests were performed by placing the samples between two rigid plates and applying the load with displacement control which is of special importance to adequately perform compressive strength tests. All tests were performed on cubic specimens with the dimensions of 40 × 40 × 40 mm^3. The test was carried out in laboratory conditions at 20 ± 2 °C and 60 ± 5 % relative humidity at all time.

All samples were heated from ambient temperature to 100, 200, 300, 400, 500, 600, 700, 800, 900 and 1000 °C in an electric furnace with a heating rate of 2 °C/min and then cooled to room temperature after samples were cured for 24 h at 40 °C. For all the samples, the maximum temperature was maintained for 2 h. The temperature versus time curve provided in Fig. 4 reveals the temperature evolution of OPC and fly ash–metakaolin geopolymer samples heated at 100, 200, 300, 400, 500, 600, 700, 800, 900 and 1000 °C, respectively. It indicates similar temperature evolution with time for the two series of samples.

Sample characterization including mass change (the ratio of mass losses of the OPC and geopolymer samples determined from the masses change before and after the heat exposure by analytical balance to initial mass of samples), shrinkage and morphology was conducted on geopolymer and OPC samples to evaluate the effects of the elevated temperature exposure.

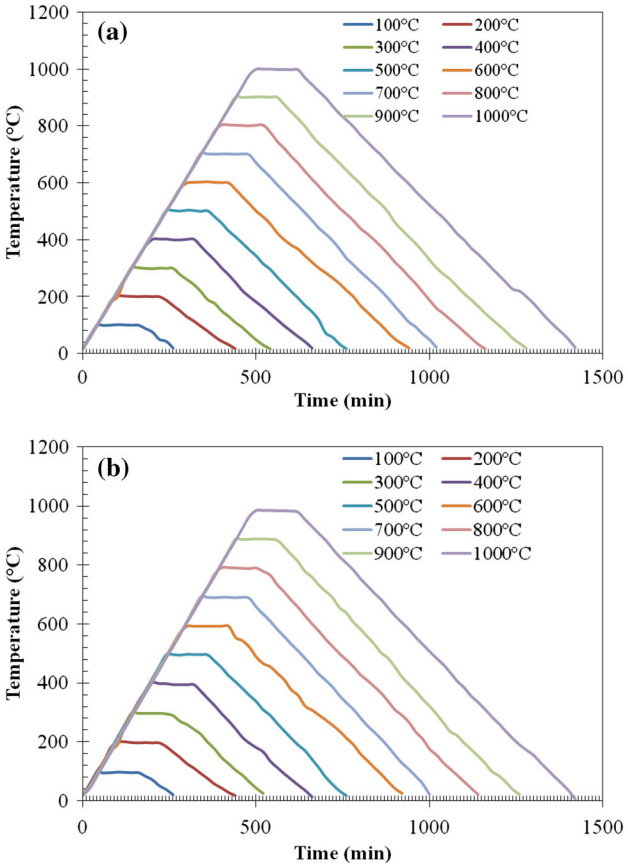

Fig. 4 Temperature evolution of geopolymer and OPC samples. **a** OPC; **b** geopolymer

Paste specimens of the size 20 × 20 × 200 mm^3 were prepared for the shrinkage test. The specimens were removed from the molds after being cured for 24 h. The prism specimens were installed onto the setup for the length change tests shown in Fig. 5 and cured in a room with constant temperature and relative humidity (20 ± 3 °C, RH = 90 ± 5 %). Length changes of the prism before and after high-temperature exposure were recorded by reading the dial gauge regularly [8]. Shrinkage was measured after pre-drying at 105 °C for 24 h to remove free water to avoid excessive shrinkage in the initial stage of the measurement. This step ensured that contact between the sample and the pushrod of the dilatometer was maintained.

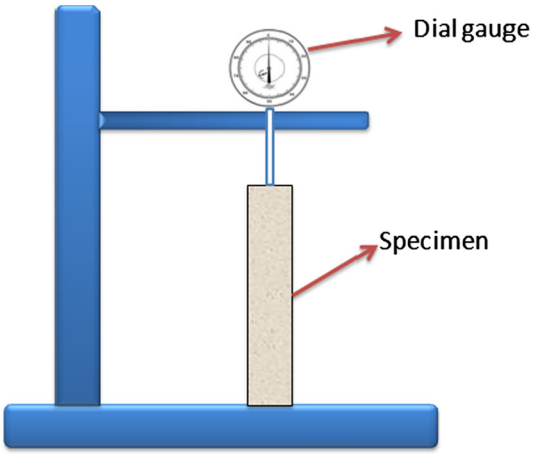

Fig. 5 Schematic diagram of the setup for testing the length change

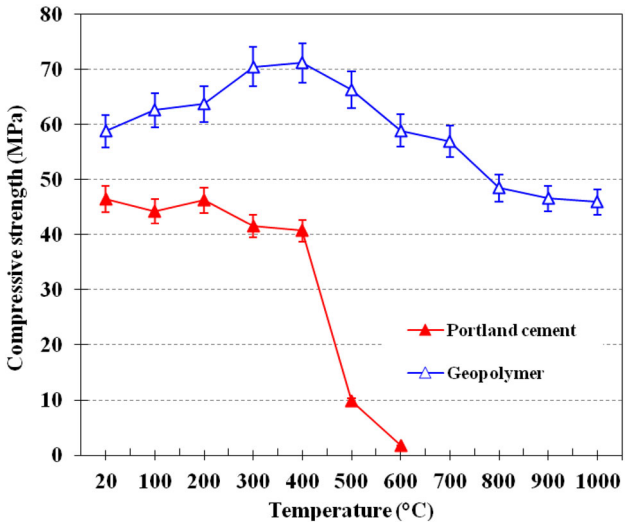

Fig. 6 Compressive strength of geopolymer and OPC pastes at various temperatures (maximum and minimum deviation values are 3.5 and 0.1 MPa, respectively)

The morphological changes that occur during thermal exposure were obtained by means of JSM-5610LV scanning electron microscope (SEM). The specimens for morphology observation were cut into prisms of about $8\times8\times2\,mm^3$.

The porosity and pore size distribution were measured using MIP with a maximum pressure of 207 MPa, and the contact angle was 140 °C. The samples were immersed in ethanol to stop hydration immediately and were crushed and dried at about 105 °C for 24 h before MIP test. For comparison, the relative properties of cement paste (CEM O 42.5) with a water/cement ratio of 0.5 was also measured.

4 Results and Discussion

4.1 Compressive Strength

The bulk density of geopolymer and OPC samples was determined by weighing following the standard procedure described in standard EN 1015-6 [9]. The filling and compaction method for fresh pastes was applied. The bulk density of samples was calculated as the mean value of two measurements rounded to the nearest $10\,kg/m^3$. Bulk density 3.10, 2.65 and 2.77 g/cm^3 was obtained for portland cement paste, fly ash-based geopolymer and metakaolin-based geopolymer, respectively.

The compressive strength of OPC and geopolymer paste specimens at 28 days after heated to 100, 200, 300, 400, 500, 600, 700, 800, 900 and 1000 °C, respectively, and cooled to room temperature was tested. Six specimens were tested at each 100 °C intervals after cooling to 20 °C, and the results are presented in Fig. 6. The results provided in Fig. 6 reveal that the OPC paste suffered a 10 % strength loss up to 400 °C followed by an abrupt loss and practically total strength loss at 600 °C, while the geopolymer paste had gained 20 % in compressive strength at 400 °C followed by a gradual decrease in strength, at 1000 °C reducing to approximately 60 % its strength at 400 °C. Thus, the compressive strength of the geopolymer attained its maximum value 72 MPa and minimum value 46 MPa at a calcination temperature of 400 °C and 1000 °C, respectively, the latter corresponding to 75 % of the strength at 20 °C. This strength deterioration of OPC is attributed to the $Ca(OH)_2$ decomposition that occurs at about 400 °C. As the temperature increases, the dehydration of portlandite, another major product in OPC pastes, generally occurs between 400 and 550 °C [10]. The rehydration of portlandite is well known to be detrimental to cement pastes, and the degree of degradation can be directly linked to the sorptivity of heat-exposed OPC pastes [11]. In geopolymers, aluminosilicate gel is the major binding phase that provides interparticle bonding, which could enhance the compressive strength [12–14] and become the main reason for the strength increase in geopolymer paste.

4.2 Shrinkage

Shrinkage of the selected geopolymers was also investigated in terms of dimensional change after exposure to elevated temperature for 2 h. Figure 7 presents the photographs of geopolymers before and after the thermal exposures. It is observed that these geopolymers get a certain degree of volume shrinkage after the thermal exposures. Actually, OPC has been shown to exhibit a higher shrinkage compared with geopolymer [15–17], which can cause severe defects when it is practically applied in cement or concrete construction.

Shrinkage results for the OPC and geopolymer samples in this work are presented in Fig. 8. All samples exhibited shrinkage up to 1000 °C due to dehydroxylation of chemi-

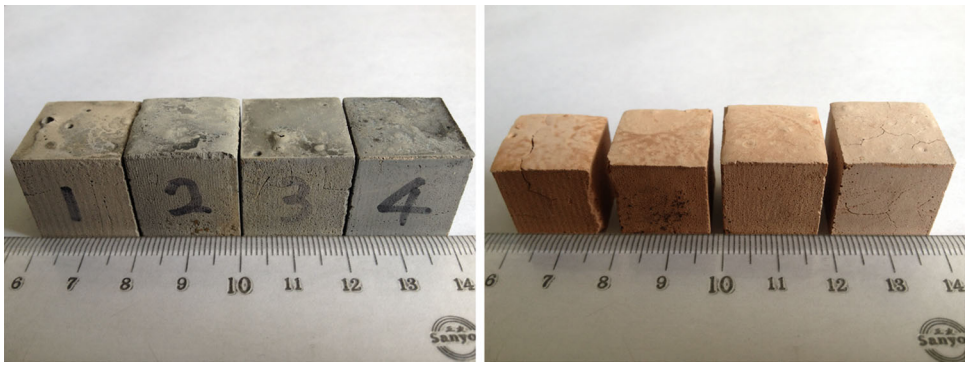

Fig. 7 Photographs of geopolymers before and after the thermal exposures

cally bound water. In a normal PC paste, pore water and crystalline hydration water can be lost from AFt- and AFm-type phases and C–S–H gel at temperatures below 300 °C [18]. As the temperature increases, the dehydration of portlandite generally occurs between 400 and 550 °C [19] and provokes a significant shrinkage effect [20]. When heated, the water trapped in concrete starts to evaporate at 300 °C, thus causing dehydration of the chemical compound C–S–H (calcium silicate hydrate) which is responsible for bonding the different concrete constituents together [21]. The dehydration of C–S–H crystals results in a decrease in strength of concrete, a process that is not reversible. At 530 °C, $Ca(OH)_2$ turns into CaO resulting in a 33 % shrinkage in volume [22]. The shrinkage is particularly evident for cement sample where dehydration of the C–A–S–H phase and C–S–H phase is believed to dominate the dilatometry profile resulting in loss of contact with the pushrod at about 1000 °C [8]. As mentioned above, length changes in the samples before and after high-temperature exposure were recorded by reading the dial gauge regularly [8]. Shrinkage leads to the decrease in length of samples, hence the loss of contact with the pushrod as shown in Fig. 5. The shrinkage for geopolymer is likely due to sintering and further geopolymerization at elevated temperature above 600 °C which is revealed by X-ray diffraction (XRD), scanning electron microscopy (SEM) and energy dispersive spectrometry (EDS) [23,24].

Polynomial trend lines were used to show the trend of shrinkage evolution in geopolymer specimens with increasing temperature. A linear relationship was found between shrinkage evolution and the elevated temperature for cement specimens. Obviously, cement exhibited evident and higher shrinkage values when compared to geopolymer pastes.

Shrinkage under practical conditions depends on loss of water from the pores, which determines how easily water may be lost from the pores. The geopolymer specimens is expected to result in a much denser matrix (see 4.4 pore size distribution) and lower porosity compared to OPC, hence an increased rigidity of the solid network, leading to a higher resistance to the shrinkage. Therefore, cement exhibited evident and higher shrinkage values when compared to geopolymer pastes.

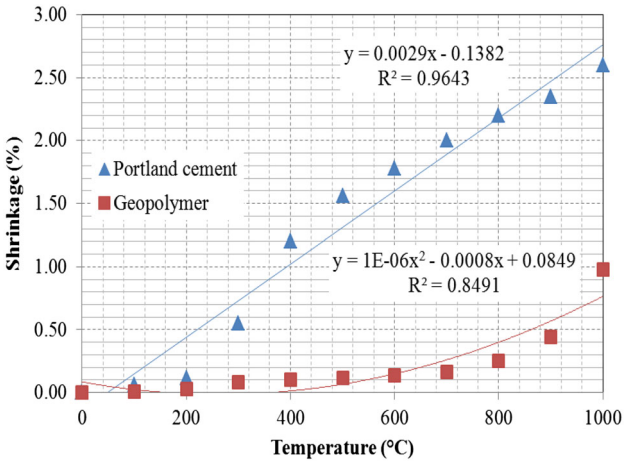

Fig. 8 Thermal shrinkage of portland cement and geopolymer paste with elevated temperature

4.3 Mass Loss

The average values of mass loss after exposure to different temperature are plotted in Fig. 9. The mass loss is nearly proportional to the temperature up to 400 and 600 °C for geopolymer and OPC paste, respectively, as observed in Fig. 9. At higher temperatures, the mass loss is constant for the geopolymer paste and could not be determined for OPC paste because of spalling of the specimens. The geopolymer shows similar mass loss curves up to 400 °C as OPC, with relatively greater mass loss for geopolymer specimen than OPC in this region. It can be seen from Fig. 9 that most of the mass loss occurs around 400 °C. The mass loss of the geopolymer specimens at 1000 °C was 3.39 %. The geopolymer microstructures became denser with the increase in fire temperature up to 400 °C as shown in Fig. 10. This change has occurred in the microstructure because of sintering and further geopolymerization with the increase in temperature [23,24]. Thus, the microstructure of geopolymer specimens remained stable after exposure to high temperature and presents less mass loss at temperatures tested above 400 °C.

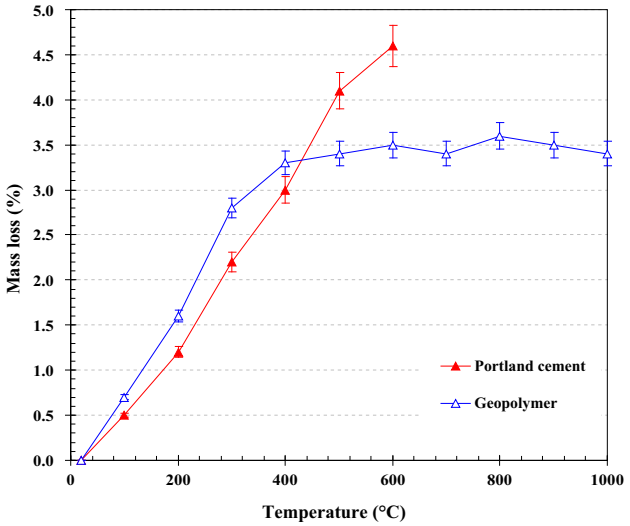

Fig. 9 Change in mass loss of geopolymer and OPC pastes with fire temperature

4.4 Pore Size Distribution

As pointed out by Diamond [25], MIP is the only available procedure that purports to cover nearly the whole range of sizes that must be tallied. The pore size distribution measurements performed by MIP of metakaolin and fly ash geopolymer samples and OPC paste are shown in Fig. 11. The results at 28 days are plotted to identify how pore size distribution changes with mix proportion. Apparent porosity of metakaolin and fly ash geopolymer samples and OPC paste is listed in Table 5. The results at 28 days followed by heating at 400 °C shown in Fig. 12 are used to assess how pore size distribution changes after heat exposure.

The comparison of metakaolin geopolymer, fly ash geopolymer and OPC paste shows that the total porosity (cumulative intrusion volume) is decreasing for geopolymer pastes compared to OPC. The porosity evolution trend can also be observed in Table 5. The differential curves of pore size distribution are almost identical between different samples. The critical pore diameters, defined as the peaks in the differential curves, giving the rate of mercury intrusion per change in pressure (differential curves) [26], did not show a significant change. However, as expected, the total pore volume in traditional OPC is higher than that in geopolymer.

Cumulative intrusion volume of OPC is higher than that of geopolymer as shown in Figs. 11a and 12a, and for the same volume of specimens, it means total porosities of the OPC samples are higher than that of the geopolymers. Combined with results in Table 5, it can be concluded that the total porosities of the OPC samples are significantly higher than the porosities of the fly ash–metakaolin-based geopolymers.

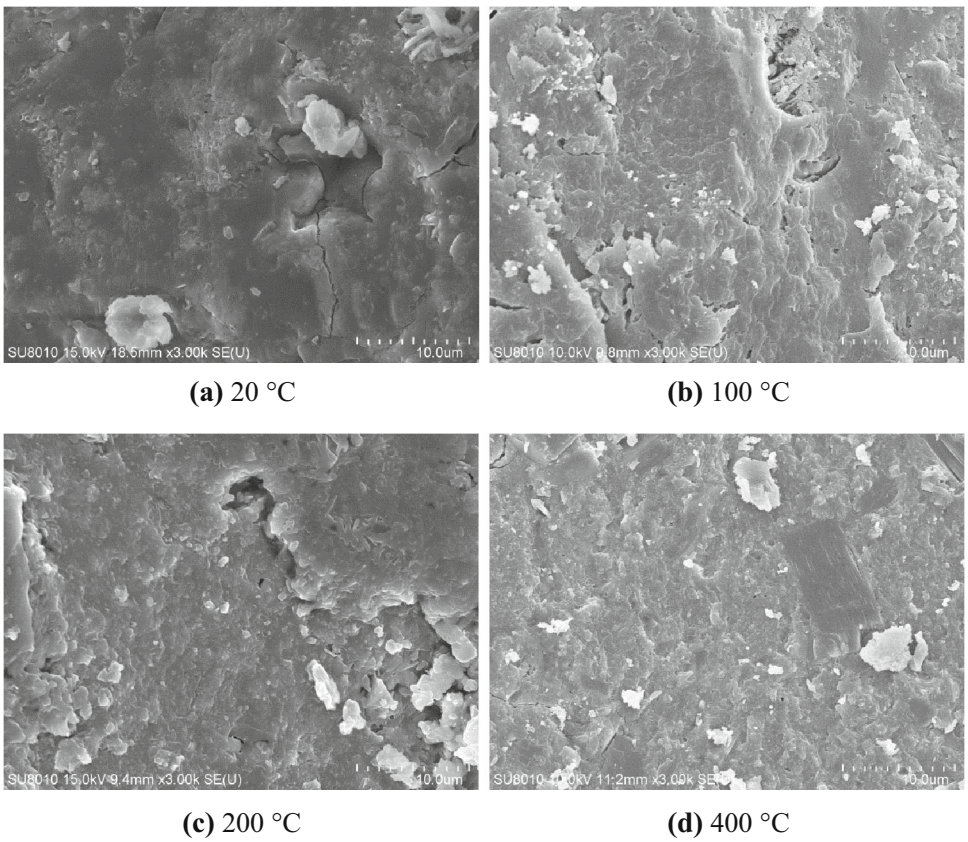

(a) 20 °C **(b)** 100 °C

(c) 200 °C **(d)** 400 °C

Fig. 10 Microstructures of geopolymer at different temperatures

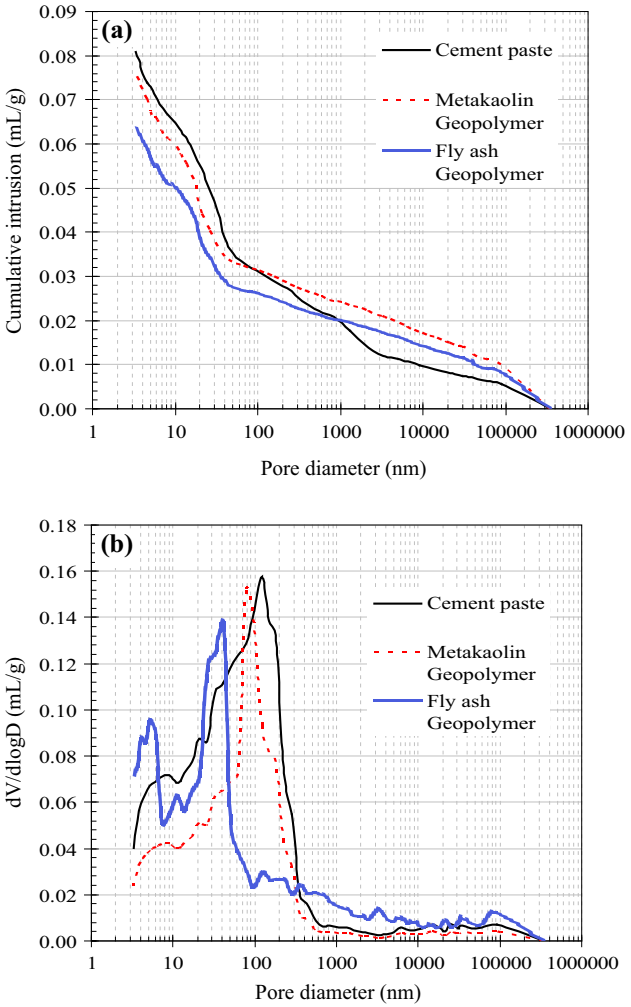

Fig. 11 Pore size distribution of metakaolin and fly ash geopolymer and OPC samples

Table 5 Apparent porosity of geopolymer and OPC paste samples

Sample	Apparent porosity (%)
Fly ash geopolymer	11.19
Metakaolin geopolymer	9.73
OPC	13.96

This is expected since the metakaolin–fly ash geopolymers contain much less liquids than OPC (water/cement ratio = 0.5). Capillary pressure is related to the pore size through the Young–Laplace equation, and effective porosity refers to the pore space in the capillary and gel pores [27]. The volume of the gel and capillary pores is considerably reduced if heating is allowed to take place [28]. The pore system left behind by liquid in the cement system tends to be larger than the pores created by partially dissolved hollow fly ash particles in the geopolymer system after heating.

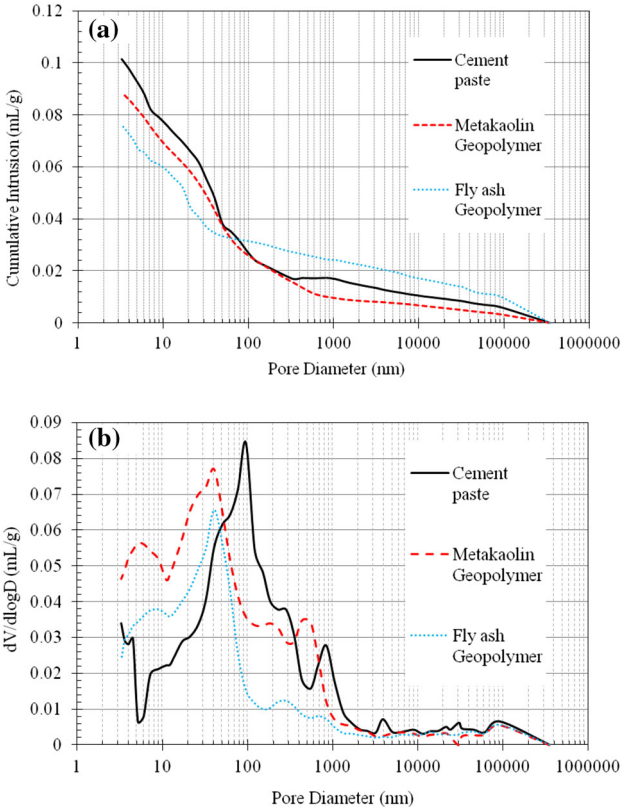

Fig. 12 Porosity and pore size distribution of geopolymer and OPC paste after heat exposure at 400 °C

5 Conclusions

1. OPC suffered strength loss after high-temperature exposure. The fly ash–metakaolin-based geopolymer gained strength up to 500 °C and lost strength at higher temperatures.
2. Polynomial trend lines were used to show the trend of shrinkage evolution in geopolymer specimens with increasing temperature. A linear relationship was found between shrinkage evolution and the elevated temperature for OPC. Cement exhibited higher shrinkage values compared to geopolymer pastes.
3. The mass loss is nearly proportional to the temperature up to 400 °C and 600 °C for geopolymer and OPC paste, respectively. At higher temperatures, the mass loss is constant for the geopolymer paste and could not be determined for OPC paste because of spalling of the specimens. The geopolymer shows similar mass loss curves up to 400 °C as OPC, with relatively greater mass loss for geopolymer specimen than that for OPC in this region.
4. The geopolymer microstructures became denser with the increase in fire temperature up to 400 °C. The comparison of metakaolin geopolymer, fly ash geopolymer

and OPC paste shows that the total porosity is decreasing for geopolymer pastes compared to OPC.

Acknowledgments This work was supported by the Fundamental Research Funds for the Central Universities (G1323511543), China University of Geosciences (Wuhan) and China Postdoctoral Science Foundation (1231512).

References

1. Temuujin, J.; Rickard, W.; Lee, M.; van Riessen, A.: Preparation and thermal properties of fire resistance metakaolin-based geopolymer-type coatings. J. Non Cryst. Solids **357**(5), 1399–1404 (2011)
2. Zhang, J.Y.; Li, S.; Wang, Y.C.; Xu, D.L.: Microstructural and strength evolutions of geopolymer composites reinforced by resin exposed to elevated temperature. J. Non Cryst. Solids **358**(3), 620–624 (2012)
3. Rickard, W.D.A.; Temuujin, J.; van Riessen, A.: Thermal analysis of geopolymer pastes synthesized from five fly ashes of variable composition. J. Non Cryst. Solids **358**(15), 1830–1839 (2012)
4. Autef, A.; Joussein, E.; Gasgnier, G.; Rossignol, S.: Role of the silica source on the geopolymerization rate: A thermal analysis study. J. Non Cryst. Solids **366**(15), 13–21 (2013)
5. Aredes, F.G.M.; Campos, T.M.B.; Machado, J.P.B.; Sakane, K.K.; Thim, G.P.; Brunelli, D.D.: Effect of cure temperature on the formation of metakaolinite-based geopolymer. Ceram. Int. **41**(6), 7302–7311 (2015)
6. Sarker, P.K.; Mcbeath, S.: Fire endurance of steel reinforced fly ash geopolymer concrete elements. Constr. Build. Mater. **90**, 91–98 (2015)
7. Pangdaeng, S.; Phoo-ngernkham, T.; Sata, V.; Chindaprasirt, P.: Influence of curing conditions on properties of high calcium fly ash geopolymer containing Portland cement as additive. Mater. Des. **53**, 269–274 (2014)
8. Yuan, X.H.; Chen, W.; Lu, Z.A.; Chen, H.G.: Shrinkage compensation of alkali-activated slag concrete and microstructural analysis. Constr. Build. Mater. **66**(15), 422–428 (2014)
9. EN 1015-6, European Standard: Methods of test for mortar for masonry-Part 6: Determination of bulk density of fresh mortar. European Committee for Standardization (CEN) (1998)
10. Shoaib, M.M.; Ahmed, S.A.; Balaha, M.M.: Effect of fire and cooling mode on the properties of slag mortars. Cem. Concr. Res. **31**, 1533–1538 (2001)
11. Mendes, A.; Sanjayan, J.G.; Gates, W.P.; Collins, F.: The influence of water absorption and porosity on the deterioration of cement paste and concrete exposed to elevated temperatures, as in a fire event. Cem. Concr. Compos. **34**, 1067–1074 (2012)
12. Palomo, A.; Grutzeck, M.W.; Blanco, M.T.: Alkali-activated fly ashes: a cement for the future. Cem. Concr. Res. **29**(8), 1323–1329 (1999)
13. Rahier, H.; van Mele, B.; Wastielsm, J.: Low-temperature synthesized aluminosilicate glasses part II rheological transformations during low-temperature cure and high temperature properties of a model compound. J. Mater. Sci. **31**(1), 80–85 (1996)
14. Duxson, P.; Lukey, G.C.; van Deventer, J.S.J.: Physical evolution of Na-geopolymer derived from metakaolin up to 1000 °C. J. Mater. Sci. **42**(9), 3044–3054 (2007)
15. Douglas, E.; Bilodeau, A.; Malhotra, V.M.: Properties and durability of alkali-activated slag concrete. ACI Mater. J. **89**(5), 509–516 (1992)
16. Wang, S.D.; Pu, X.C.; Scrivener, K.L.; Pratt, P.L.: Alkali-activated slag cement and concrete: a review of properties and problems. Adv. Cem. Res. **7**(27), 93–102 (1995)
17. Collins, F.; Sanjayan, J.G.: Microcracking and strength development of alkali activated slag concrete. Cem. Concr. Res. **23**(4), 345–352 (2001)
18. Rostasy, F.S.; Weib, R.; Wiedemann, G.: Changes of pore structure of cement mortars due to temperature. Cem. Concr. Res. **10**, 157–164 (1980)
19. Shoaib, M.M.; Ahmed, S.A.; Balaha, M.M.: Effect of fire and cooling mode on the properties of slag mortars. Cem. Concr. Res. **31**, 1533–1538 (2001)
20. Yuzer, N.; Akoz, F.; Dokuzer Ozturk, L.: Compressive strength–color change relation in mortars at high temperature. Cem. Concr. Res. **34**, 1803–1807 (2004)
21. Georgali, B.; Tsakiridis, P.E.: Microstructure of fire-damaged concrete. A case study. Cem. Concr. Compos. **27**, 255–259 (2005)
22. Yüzer, N.; Aköz, F.; Dokuzer Öztürk, L.: Compressive strength–color change relation in mortars at high temperature. Cem. Concr. Res. **34**, 1803–1807 (2004)
23. Ranjbar, N.; Mehrali, M.; Alengaram, U.J.; Metselaar H.S., C.; Jumaat, M.Z.: Compressive strength and microstructural analysis of fly ash/palm oil fuel ash based geopolymer mortar under elevated temperatures. Constr. Build. Mater. **65**, 114–121 (2014)
24. Abdulkareem, O.A.; Al Bakri, A.M.M.; Kamarudin, H.; Nizar, I.K.; Saif, A.A.: Effects of elevated temperatures on the thermal behavior and mechanical performance of fly ash geopolymer paste, mortar and lightweight concrete. Constr. Build. Mater. **50**, 377–387 (2014)
25. Diamond, S.: Mercury porosimetry: an inappropriate method for the measurement of pore size distributions in cement-based materials. Cem. Concr. Res. **30**(10), 1517–1525 (2000)
26. Akkaya, Y.; van Breugel, K.; Shah, S.P.: Rheological model for self-consolidating concrete. ACI Mater. J. **99**(6), 549–559 (2002)
27. Zhang S., P.; Zong, L.: Evaluation of relationship between water absorption and durability of concrete materials. Adv. Mater. Sci. Eng. **2014**, 373–380 (2014)
28. Lai, W.L.; Tsang, W.F.: Characterization of pore systems of air/water-cured concrete using ground penetration radar(GPR) through continuous water injection. Constr. Build. Mater. **22**, 250–256 (2008)